Volume 6
Number 15
7 August 2024
Pages 3685–3980

Nanoscale Advances

rsc.li/nanoscale-advances

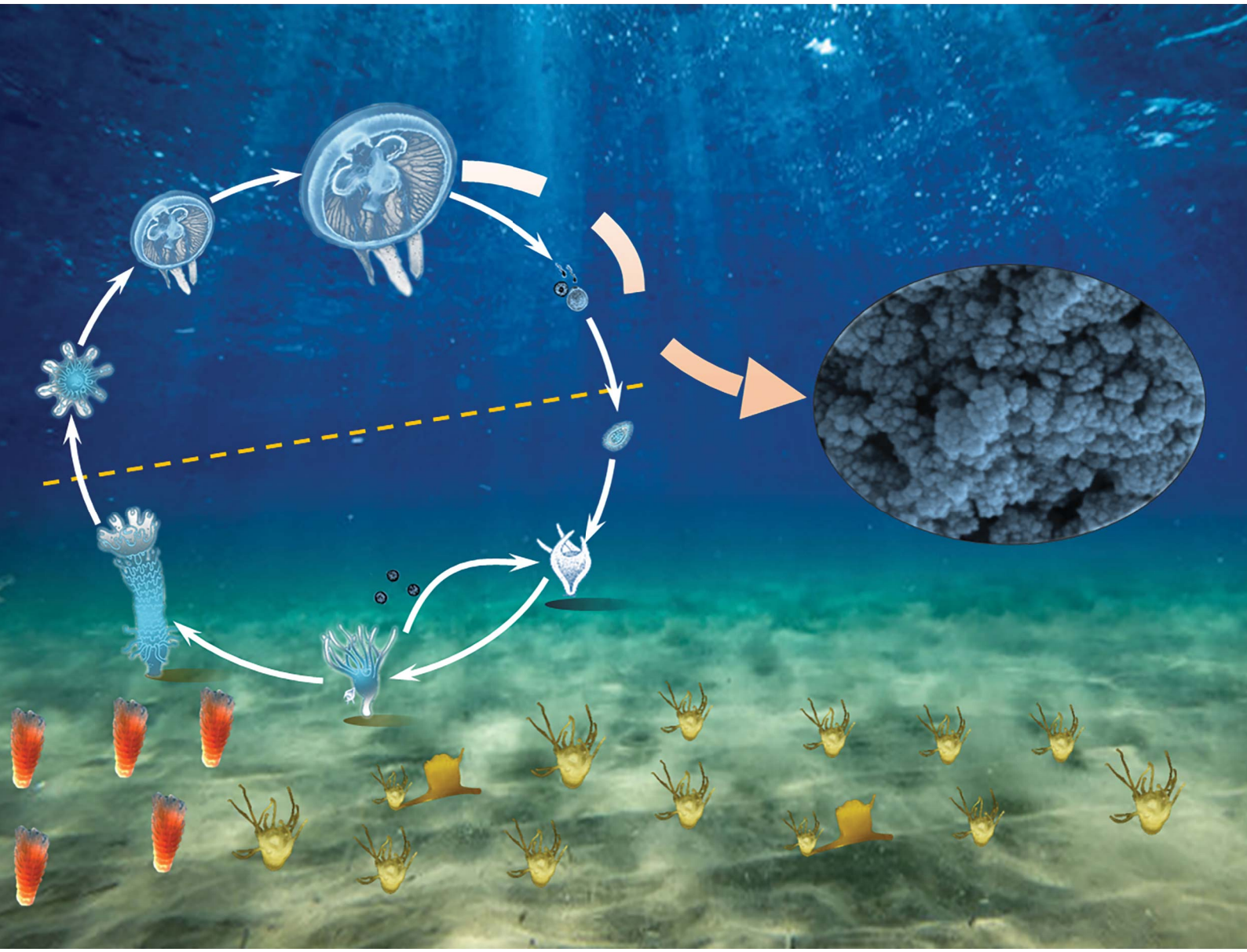

ISSN 2516-0230

ROYAL SOCIETY OF CHEMISTRY

PAPER

Song Feng, Lingchen Liu, Jianing Lin, Bin Zhang *et al.*
Bio-inspired synthesis of N-doped TiO_2/C nanocrystals using jellyfish mucus with high visible-light photocatalytic efficiency

NCNST

Nanoscale Advances

ROYAL SOCIETY OF CHEMISTRY

PAPER

View Article Online
View Journal | View Issue

Cite this: *Nanoscale Adv.*, 2024, **6**, 3759

Bio-inspired synthesis of N-doped TiO_2/C nanocrystals using jellyfish mucus with high visible-light photocatalytic efficiency†

Song Feng, *[ab] Lingchen Liu,*[cg] Jianing Lin,*[de] Ziwei Wang,[f] Jinzeng Gu,[de] Lutao Zhang,[de] Bin Zhang*[c] and Song Sun[ab]

Non-metal doping of titanium dioxide (TiO_2) has been widely investigated, because it can facilely improve the optical response of TiO_2 under visible light excitation in environmental pollution treatments. In the ongoing efforts, however, little consideration has been given to the use of harmful marine organisms as dopants. Here, we employed the natural mucus proteins of the large harmful jellyfish *Aurelia coerulea* and *Nemopilema nomurai*, which have frequently bloomed in East Asian marginal seas in recent decades, to synthesize mesoporous nitrogen-doped TiO_2 nanocrystals modified with carbon (N–TiO_2/C) by a simple hydrothermal method. These nanocrystals were composed of predominantly anatase phase and a small amount of brookite phase TiO_2. Their mesoporous structures changed with the variation of the volume ratio of jellyfish mucus added to tetrabutyl titanate (TBT). At the same ratio, larger surface area and pore volume but smaller pore size were observed in N–TiO_2/C nanocrystals from *N. nomurai* rather than *A. coerulea*. Nitrogen was determinately doped into the lattice of the prepared nanocrystals and the carbon species were modified on their surfaces, which narrowed the band gap, facilitated the separation of photogenerated electron–hole pairs and favored the absorption of visible light, thus improving their visible light photocatalytic activity. The photocatalytic degradation efficiency of Rhodamine B (RhB) under visible light irradiation first increased and then decreased with the gradual increase of the volume ratio of jellyfish mucus proteins to TBT. The maximum reached 97.52% in 20 min from N–TiO_2/C nanocrystals synthesized using *N. nomurai* mucus at the volume ratio of 4 : 1, which showed a remarkably strong visible light absorption, lower band gap energy and smaller electron transfer resistance. These N–TiO_2/C nanocrystals also had a relatively stable crystal structure in multiple degradation reactions. The main active species including superoxide radicals ($^{\bullet}O_2^-$), photogenerated holes (h^+) and hydroxyl radicals ($^{\bullet}OH$) were found to play a major role in the degradation process of RhB. This study highlights the potential high-value reapplication of harmful jellyfish mucus as a natural organic matrix in fabricating advanced materials with optimized functional properties.

Received 11th April 2024
Accepted 19th June 2024

DOI: 10.1039/d4na00309h

rsc.li/nanoscale-advances

1 Introduction

Photocatalysis by semiconductors has been receiving widespread attention in environmental pollution control. It has been considered as a green chemistry technology that could degrade some environmental pollutants such as organic pollutants, microplastics, *etc.*[1–7] Among numerous semiconductor materials, titanium dioxide (TiO_2) shows good potential in practical engineering applications due to its strong oxidation ability, and stable and non-toxic chemical properties.[8] However, TiO_2 anatase and rutile can only be stimulated by UV light absorption to generate electronic transitions in photocatalytic reactions because of their large band gap (3.2 eV and 3.0 eV, respectively). The high recombination rate of the charge carriers might result in relatively low degradation efficiency and high energy consumption.[9–11] In natural solar radiation, the UV light spectrum only accounts for approximately 4%, while most of the

[a]CAS Key Laboratory of Marine Ecology and Environmental Sciences, Institute of Oceanology, Chinese Academy of Sciences, Qingdao 266071, China. E-mail: fengsong@qdio.ac.cn
[b]College of Marine Sciences, University of Chinese Academy of Sciences, Qingdao 266400, China
[c]School of Architecture and Civil Engineering, Xihua University, Chengdu 610039, China. E-mail: lingchen2773@163.com; 0720060057@mail.xhu.edu.cn
[d]Institute of Eco-Environmental Forensics, Shandong University, Qingdao 266237, China. E-mail: linjianing@sdu.edu.cn
[e]Laboratory for Marine Ecology and Environmental Science, Qingdao Marine Science and Technology Center, Qingdao 266237, China
[f]Liaoning University, Shenyang 110036, China
[g]Bureau of Natural Resources of Daan District, Zigong 643000, China

† Electronic supplementary information (ESI) available. See DOI: https://doi.org/10.1039/d4na00309h

spectrum consists of visible light.[12] Therefore, studies on the improvement of TiO_2 visible-light efficiency have become one of the hot topics in the practical treatment of environmental pollution.

Some efforts have been made to synthesize a modified TiO_2 photocatalyst with high reactivity under visible light by narrowing its band gap or forming an interstitial gap.[9,13–16] An effective method is the doping of TiO_2 with non-metal elements (*e.g.*, C, N, S, *etc.*). Compared to metal-doped TiO_2, which usually exhibits poor thermal stability and easily suffers from photo-corrosion,[11,17] non-metal doping has been reported to yield higher efficiency in the process of transition from the ultraviolet of TiO_2 to visible photocatalysis, since the states of these modified TiO_2 nanocrystals prepared are close to the edge of the valence band with minimized recombination.[11,18] A variety of nitrogen and carbon sources (*e.g.*, glycine, guanidine hydrochloride, *etc.*) have been applied to synthesize C and N modified-TiO_2 nanocrystals by numerous approaches, including sol–gel methods, hydrothermal methods, pyrolysis, calcination, *etc.*[19–23] For example, Wang *et al.* (2012) used L-lysine as the dopant to prepare N-doped TiO_2 nanocrystals sensitized with C (N–TiO_2/C) by a one-pot hydrothermal treatment.[24] The photocatalytic activity of the as-obtained N–TiO_2/C improved well because the N-doping narrowed the band gap and the C-modification heightened the visible light harvesting and accelerated the separation of the photogenerated electron–hole pairs.[24] Apart from the chemical raw materials, C, N modified-TiO_2 nanocrystals are actively obtained by the application of some natural bioorganic materials as dopants at present.[23,25] By utilizing the extrapallial fluid proteins of mussels as the doping source, Zeng *et al.* (2015) fabricated N-doped TiO_2 photocatalysts with high visible-light photocatalytic activity.[26] Although the utilization of bioorganic matter from nature as a non-metal element source was considered to be not only able to produce modified TiO_2 photocatalysts in a single process, but also beneficial to reduce the production costs and pollution,[8,25] currently reported available sources are still few in the synthesis of C, N modified TiO_2,[23,25] especially with regard to harmful marine organisms (Table S1†).

Jellyfish is a class of gelatinous invertebrates with a body plan characterized by a high water and low carbon content,[27] most of which live in the ocean. In recent decades, jellyfish blooms have frequently occurred around the world (Fig. S1†), causing severe ecological and socio-economic damages such as stinging bathers, clogging the cooling water intakes of coastal nuclear/coal-fired power plants, disturbing normal fishery production, threatening fishery resources, impacting marine ecosystem structure, *etc.*[28,29] Therefore, the prevention and control of jellyfish blooms have become an important topic in the global jellyfish research, among which the reuse of harmful jellyfish is a popular direction. At present, many large harmful jellyfish such as *Aurelia coerulea* and *Nemopilema nomurai*, which frequently bloom in large numbers in the East Asian marginal seas[30] (Fig. S2†), have been reported to have abundant mucus on their body surfaces, secreting more when stimulated.[31] Previous studies have found that jellyfish mucus has the potential to remove nanoparticles from contaminated water by capturing them in water.[32] Since jellyfish mucus is generally rich in many types of proteins including metalloproteinase,[33,34] it is not clear whether they could be used as a natural doping source to regulate the functional properties of TiO_2. Therefore, in order to explore a new strategy for the recycle of harmful jellyfish, mesoporous N–TiO_2/C nanocrystals were developed at a low temperature by a simple "one-pot" method by using the mucus proteins of large jellyfish *A. coerulea* and *N. nomurai* as the natural doping sources in this study. The obtained N–TiO_2/C nanocrystals exhibited high visible-light photocatalytic activity for Rhodamine B (RhB) degradation.

2 Materials and methods

2.1 Extraction of jellyfish mucus proteins

Fresh medusae of *A. coerulea* and *N. nomurai* with the respective umbrella diameters of approximately 10–15 cm and 50–80 cm were captured in the coastal waters of Qingdao, China, in June and August, respectively. The entire medusae in *A. coerulea* and partial oral arms in *N. nomurai* were rinsed thoroughly with fresh seawater filtered through a 0.45 μm hybrid fiber membrane, respectively. Afterwards, their mucus was collected into 50 mL centrifuges on ice using funnels containing a layer of medical gauze (Fig. S3†). The obtained mucus was then centrifuged at 4000–12 000 rpm for 10 min to remove impurities. The supernatant was extracted using a disposable syringe and the protein concentration was analyzed through the Bradford Assay (Bradford, 1976). The protein bands were detected by 10% sodium dodecyl sulphate-polyacrylamide gel electrophoresis (SDS-PAGE). The mucus proteins were finally diluted or concentrated to the desired concentration (600 μg mL^{-1}, Fig. S4†) by referring to the reports of Zeng *et al.* (2015).[26]

2.2 Synthesis of TiO_2 materials

The schematic of the synthesis process of modified TiO_2 nanocrystals by using proteins of *A. coerulea* and *N. nomurai* mucus as the dopants is described in Fig. 1. Three volumes of mucus proteins (10 mL, 20 mL and 30 mL) in *A. coerulea* and *N. nomurai* were separately dropped into 5 mL of tetrabutyl titanate (TBT, 97%, Sigma-Aldrich) in a 50 mL beaker with the volume ratios of 2 : 1, 4 : 1 and 6 : 1. They were constantly stirred for 2 h at 300 rpm min^{-1}. After 4 h mineralization without stirring, the mixture (*i.e.*, jellyfish mucus and TBT) was transferred to a Teflon-lined autoclave and preheated at 50 °C for 30 min. Then temperature was adjusted to 150 °C at a heating rate of 5 °C min^{-1}. The heat treatment process at 150 °C lasted for 12 h. When the reactor naturally cooled to the room temperature, a mixture including a light brown precipitate and a liquid appeared (Fig. S5a†). Afterwards, the precipitate was collected by firstly centrifugation at 4000 rpm min^{-1} for 10 min, followed by separately washing with anhydrous ethanol and distilled water 3 times, and drying at 55 °C for 12 h. The modified TiO_2 nanocrystals were finally obtained after thorough grinding (Fig. S5b†), which are

denoted as JAT for *A. coerulea* and JNT for *N. nomurai*. According to the volume ratio between the mucus proteins utilized and TBT, the 6 TiO_2 nanocrystals are abbreviated as JAT-2, JAT-4 and JAT-6, as well as JNT-2, JNT-4 and JNT-6, respectively.

2.3 Characterization of materials

The morphology of the obtained modified TiO_2 samples was characterized by scanning electron microscopy (SEM, TESCAN MIRA LMS) and transmission electron microscopy (TEM, JEOL JEM 2100F). The crystalline phase was analyzed by X-ray diffraction (XRD, Rigaku SmartLab SE) with Cu-Kα radiation (operation voltage of 40 kV and current of 40 mA). The scan was conducted between 10 and 80° at the scanning rate of 2° per min. The nitrogen adsorption–desorption isotherms were measured using an automatic adsorption unit (Quantachrome Autosorb IQ) at 196 °C after degassing the samples for 8 h. The pore surface area, volume and diameter distribution were determined by the Barrett–Joyner–Halenda (BJH) method. X-ray photoelectron spectroscopy (XPS, Thermo Scientific K-Alpha) was used to know the surface elemental composition, chemical bonding valence states and charge distribution of the samples. The UV-vis absorption spectra of the samples were recorded using a Shimadzu UV-3600i Plus equipped with an integrating sphere attachment, using $BaSO_4$ as the reference in the wavelength range of 200–800 nm. Photoluminescence (PL) spectra were obtained (Edinburgh FLS1000) with a 300–700 nm excitation wavelength. The active radicals during the photocatalytic reaction process were identified using an electron paramagnetic resonance spectrometer (ESR, Bruker EMXplus-6/1) at the magnetic field strength of 3510G. Electrochemical impedance spectroscopy (EIS) was performed using a CHI760E.

2.4 Photocatalytic activity measurement

The photocatalytic activity of the samples was evaluated by the degradation of Rhodamine B (RhB) dye under visible-light irradiation. A 500 W mercury lamp equipped with a 400 nm filter was used as the light source. 10 mg of the sample was added into 10 mL RhB (0.01 mM) aqueous solution. After stirring for 30 min

Fig. 1 Schematic of the synthetic process of nitrogen-doped TiO_2 nanocrystals modified with carbon (N–TiO_2/C) by using proteins of the large harmful jellyfish *Aurelia coerulea* and *Nemopilema nomurai* mucus as dopants (MA: marker, ACS: *A. coerulea* mucus, NNS: *N. nomurai* mucus).

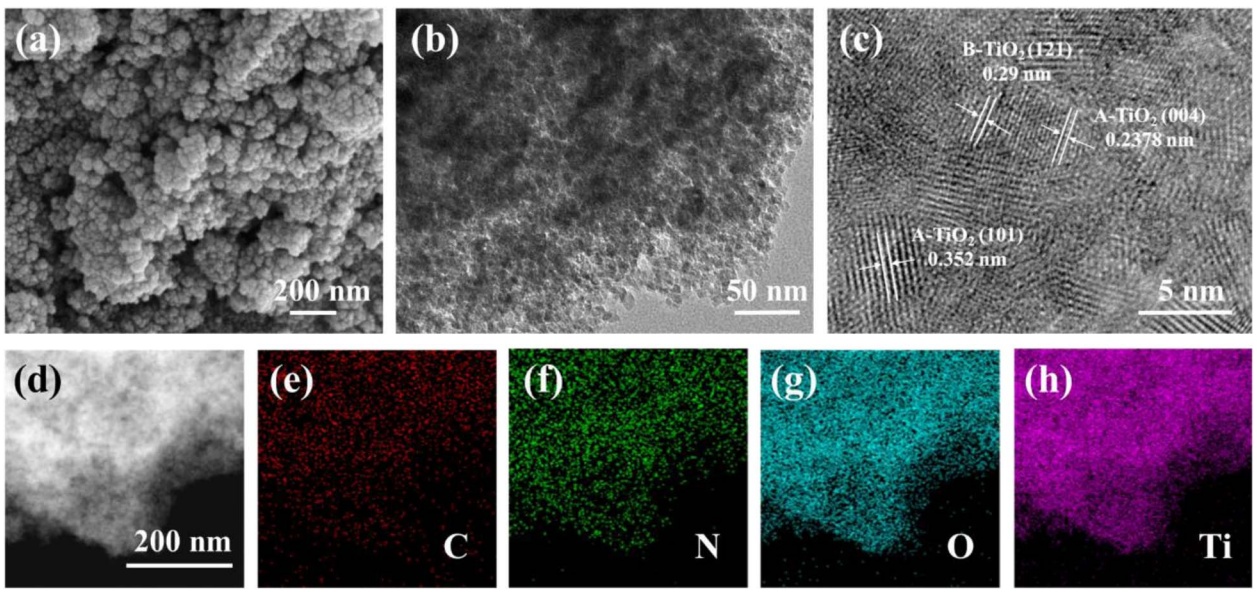

Fig. 2 SEM (a) and HRTEM (b and c) images and EDS elemental mappings (d–h) for JAT-4 nanocrystals.

in the dark, the solution was exposed to visible light. 1 mL solution was taken out using a pipette every 5 min and the supernatant was obtained by centrifugation. The concentration of the degradation solution was determined by the absorbance at 554 nm using a microplate reader. The degradation rate (D, %) of RhB was calculated as follows, eqn (1):

$$D = (C_0 - C_t)/C_0 \times 100\% \quad (1)$$

where C_0 (mmol L^{-1}) is the initial RhB concentration (ppm), and C_t (mmol L^{-1}) is the RhB concentration at time t.

In order to better evaluate the reusability and stability of the prepared photocatalysts, recycle experiments under the same conditions were conducted. After each cycle experiment, the photocatalyst was repeatedly washed with ultrapure water and anhydrous ethanol, and then placed in a beaker and boiled with ultrapure water to remove residual organic molecules. Subsequently, the photocatalyst was dried at 60 °C, and the above experiment was repeated three times.

3 Results and discussion

3.1 Morphology and pore analysis of photocatalysts

The SDS-PAGE electrophoresis map showed that *A. coerulea* mucus and *N. nomurai* mucus were rich in various kinds of proteins as previously reported[31,32] (Fig. 1). The protein bands were mainly distributed at 40–50 kDa, 50–70 kDa and 70–150 kDa in *A. coerulea*, and 15–35 kDa and 40–50 kDa in *N. nomurai*. By using *A. coerulea* and *N. nomurai* mucus as dopants, the 3D network of structured TiO_2 was achieved compared to pristine TiO_2.[26] The building units of the 6 prepared TiO_2 nanocrystals (3 JAT and 3 JNT) showed porous nanostructures resembling a "cauliflower" in the SEM characterization (Fig. 2 and 3a). This structure, which is similar to the "nanoflowers" reported by Zhou (2021),[35] may be conducive to the adsorption of pollutants and absorption of light, thereby enhancing the photocatalytic activity of the materials. The average size of the JAT and JNT nanostructures was

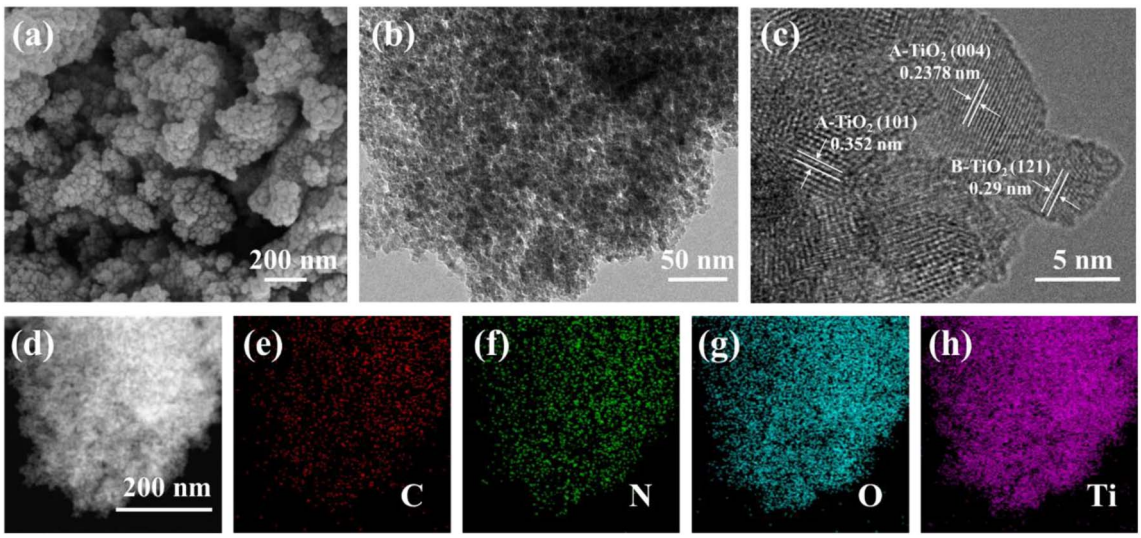

Fig. 3 SEM (a) and HRTEM (b and c) images and EDS elemental mappings (d–h) for JNT-4 nanocrystals.

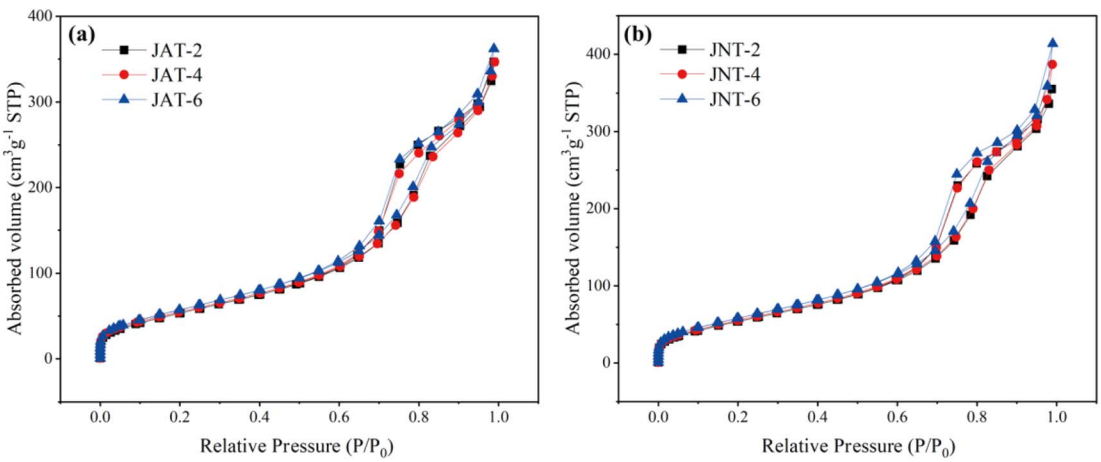

Fig. 4 N_2 adsorption–desorption isotherms of JAT (a) and JNT (b) nanocrystals at different volume ratios of the mucus proteins utilized and TBT.

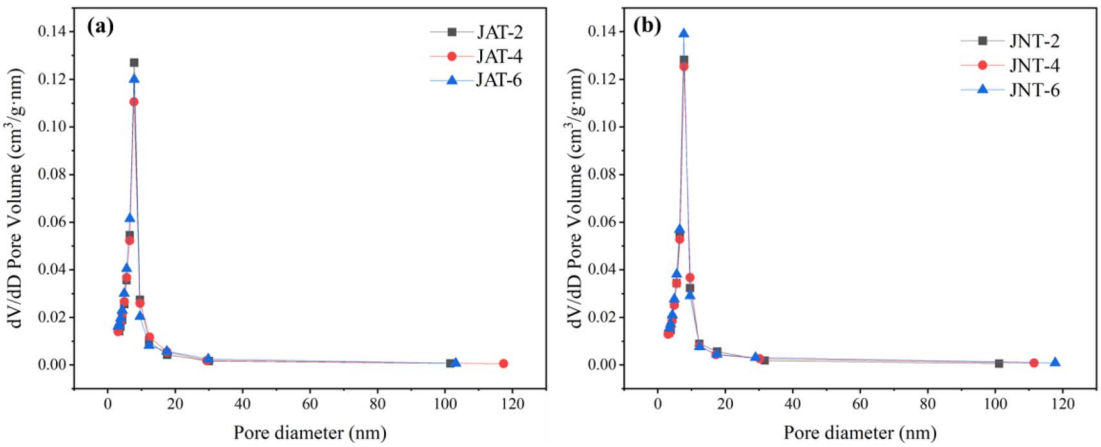

Fig. 5 Corresponding BJH pore size distribution curve of JAT (a) and JNT (b) nanocrystals.

Table 1 Surface area, pore volume and pore size of JAT (a) and JNT (b) nanocrystals at different volume ratios of their mucus proteins utilized and TBT

Jellyfish species	Photocatalyst	S_{BJH} (m^2 g^{-1})	Pore volume (cm^3 g^{-1})	Pore size (nm)
Aurelia coerulea	JAT-2	237.887	0.545	7.841
	JAT-4	236.802	0.543	7.788
	JAT-6	250.189	0.568	7.831
Nemopilema nomurai	JNT-2	245.225	0.560	7.778
	JNT-4	249.036	0.610	7.783
	JNT-6	258.772	0.649	7.722

estimated to be approx. 5 nm. The HRTEM images also clearly demonstrated that the lattice fringes with the interplanar spacing of 0.352 nm, 0.2378 nm and 0.29 nm corresponded well to the (101) and (104) planes of anatase TiO_2 (JCPDS # 86-1157), and the (121) plane of brookite TiO_2 (JCPDS # 29-1306), respectively (Fig. 2 and 3b and c), which indicated that the 6 synthesized TiO_2 nanocrystals were composed of anatase and brookite phases. The EDS elemental mappings suggested that the four elements Ti, O, N, and C were uniformly distributed throughout the entire materials (Fig. 2 and 3d–h), preliminarily indicating that N and C elements modified the TiO_2 nanocrystals according to previous studies.[36,37]

The porous structures of JAT and JNT nanocrystals were also confirmed by N_2 adsorption–desorption isotherms and the corresponding BJH analysis. From Fig. 4, the N_2 isotherms of JAT and JNT nanocrystals could be attributed to type IV isotherms, suggesting that they were typical of mesoporous materials according to the IUPAC classification. Their mesoporous hysteresis loops belonged to the H3 type, which appeared at a relative pressure ranging from 0.7 to 0.9. The mesoporous materials usually have the regular mesoporous channels, which are beneficial for the light scattering inside to enhance the light harvesting.[24,35,38] The corresponding pore size distributions of JAT and JNT nanocrystals are shown in Fig. 5. Their surface areas, pore sizes and pore volumes are given in Table 1. It can be seen that the surface area, pore volume and average pore size of JAT nanocrystals first decreased and then increased as the added volume of *A. coerulea* mucus increased. In contrast, the surface area and pore volume gradually increased with the added volume of *N. nomurai* mucus for JNT nanocrystals, however, the average pore size showed an initial increase followed by a decrease. At the same mucus volume, the surface area and pore volume of JNT nanocrystals were larger than those of JAT nanocrystals, but the pore size became smaller. This indicated that JNT nanocrystals may be able to provide more photocatalytic reaction sites for the adsorption of reactant molecules, thus in favor of enhancing the photocatalytic activity.

3.2 Phase and composition analysis of photocatalysts

Fig. 6 shows the similar X-ray diffraction (XRD) patterns of JAT and JNT nanocrystals. The diffraction peaks were exhibited at 25.32°, 37.86°, 48.06°, 54.62°, 55.09° and 62.96°, which agreed with the (101), (004), (200), (105), (211) and (204) crystal planes of anatase TiO_2 (JCPDS # 86-1157), respectively. The diffraction peak at $2\theta = 30.81°$ could be indexed to the (121) crystal plane of brookite TiO_2 (JCPDS # 29-1306). The broadening of the diffraction peaks of anatase was indicative of the small size of the obtained nanocrystals.[24] The low intensity of the peak

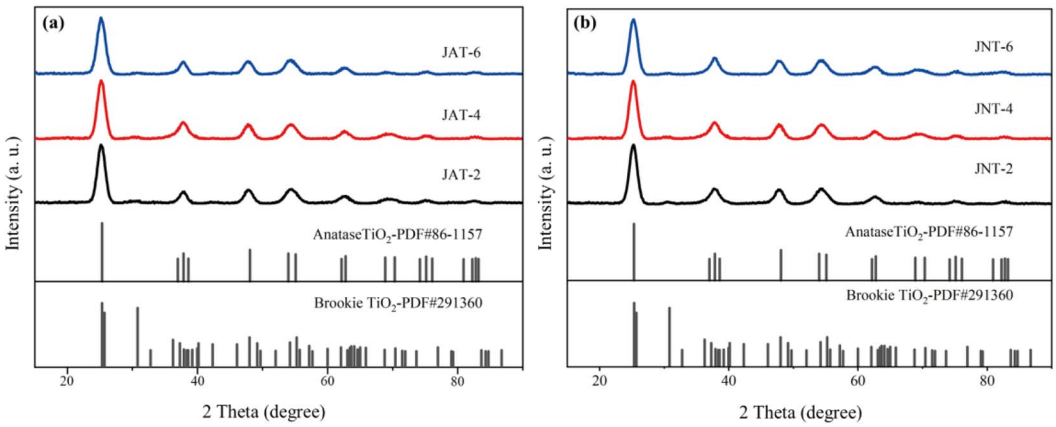

Fig. 6 X-ray diffraction patterns of JAT (a) and JNT (b) nanocrystals at different volume ratios of their mucus proteins utilized and TBT.

referred to brookite implied its relatively low amount in these nanocrystals as previously reported,[16] which may be because some biological proteins could control the crystalline phase and significantly prevent the formation of brookite.[26] Combined with the results of HRTEM, it can be deduced that the synthesized JAT and JNT nanocrystals were a mixed phase structure composed of the dominating anatase phase and a small amount of brookite phase TiO_2. Their coexistence may improve the photocatalytic efficiency.[26]

XPS spectroscopy was used to analyze the surface elemental composition, chemical valence states and charge distribution of JAT and JNT nanocrystals. The binding energies obtained in XPS analysis were corrected by referring to the peak of C1s (284.8 eV). Here the JAT-4 and JNT-4 nanocrystals were taken as an example. Four elemental peaks of Ti 2p, O 1s, C 1s, and N 1s were detected in the survey spectrum of JAT-4 and JNT-4 nanocrystals (Fig. 7 and 8a), suggesting that these four elements were present in the TiO_2 nanocrystals prepared in this study. Two peaks of Ti $2p_{1/2}$ and Ti $2p_{3/2}$ were found at 464.2 eV and 458.5 eV, respectively, with a decrease of approximately 0.3–0.4 eV compared to the pure TiO_2 (ref. 16 and 24) (Fig. 7 and 8b). This may be attributed to the formation of Ti–N bonds by the partial replacement of O^{2-} with N^{3-}, which resulted in an increase in the electron density on Ti ions owing to the introduction of the smaller electronegativity of N ions.[24,39] Ti^{4+} ions were thus partially transformed into Ti^{3+}ions by the reduction reaction and the binding energies of Ti 2p decreased correspondingly. The results preliminarily implied that nitrogen was incorporated into the lattice and substituted for oxygen in these obtained nanocrystals. The O 1s spectrum showed three peaks, which were located around 529.8 eV, 531.2 eV and 532.2 eV, respectively (Fig. 7 and 8c). The peak at 529.8 eV was characteristic of the lattice oxygen of TiO_2.[24,39,40] The other two weak energy peaks could be ascribed to OH groups and oxygen adsorbed in water, respectively.[16,40,41]

For JAT-4 and JNT-4 nanocrystals, five peaks appeared in the N 1s spectrum at 395–398 eV, around 400 eV and 401–405 eV, respectively (Fig. 7 and 8d). The two N 1s peaks at 395–398 eV could be attributed to the characteristic peaks of the Ti–N–Ti linkages, further confirming that the nitrogen atom was substitutionally doped into the TiO_2 lattice for these prepared nanocrystals.[42–46] The N 1s peak located around 400 eV was ascribed to the Ti–O–N bonds, which may come from the interstitial N as previously reported.[24,26] The other two peaks at 401–405 eV could be assigned to the nitrogen oxides (NO_x)[45] and nitrogen hydrides (NH_x)[46] adsorbed by TiO_2, respectively. Because the electronegativity of O atom was larger than that of the N atom, the electron density around N decreased in comparison to that in the TiN crystal when the nitrogen was substituted for the oxygen in the initial O–Ti–O structure.[43,44] Thus, N 1s binding energy appeared higher in the O–Ti–N environment than in the N–Ti–N environment. The relative atomic concentration of N in the JAT-4 and JNT-4 nanocrystals was estimated to be 0.63 atom% according to XPS data, respectively.

Three peaks at binding energies of 284.8, 286.3, and 288.3 eV were observed in the C 1s XPS spectra (Fig. 7 and 8e). The dominant peak at 284.8 eV was attributed to the residual element carbon formed by calcination in air, which could not be eliminated.[16,22,47–49] The second peak at 286.3 eV was ascribed to the existence of C–O–C bonds from the carbon oxygen complex adsorbed on the surface of nanocrystals.[22,47–49] The lowest peak at 288.3 eV was from the formation of Ti–O–C bonds.[22,47–49] No C1s peak at 281 eV can be observed in Fig. 7 and 8e, which indicated that no carbon was doped into the lattice of JAT-4 and JNT-4 nanocrystals.[22,49–51] Thus, it was inferred that the carbon was modified on the surfaces of both nanocrystals to form the carbonaceous layers *via* Ti–O–C and Ti–OCO bonds as reported previously.[22,47] This structure is beneficial for the charge separation, and maintains the high reactivity of the photogenerated electrons and holes by taking up photogenerated electrons.[22,51–53] Besides, the carbon in these N–TiO_2/C nanocrystals acts as a surface sensitizer to absorb more visible light to improve the photocatalytic efficiency.

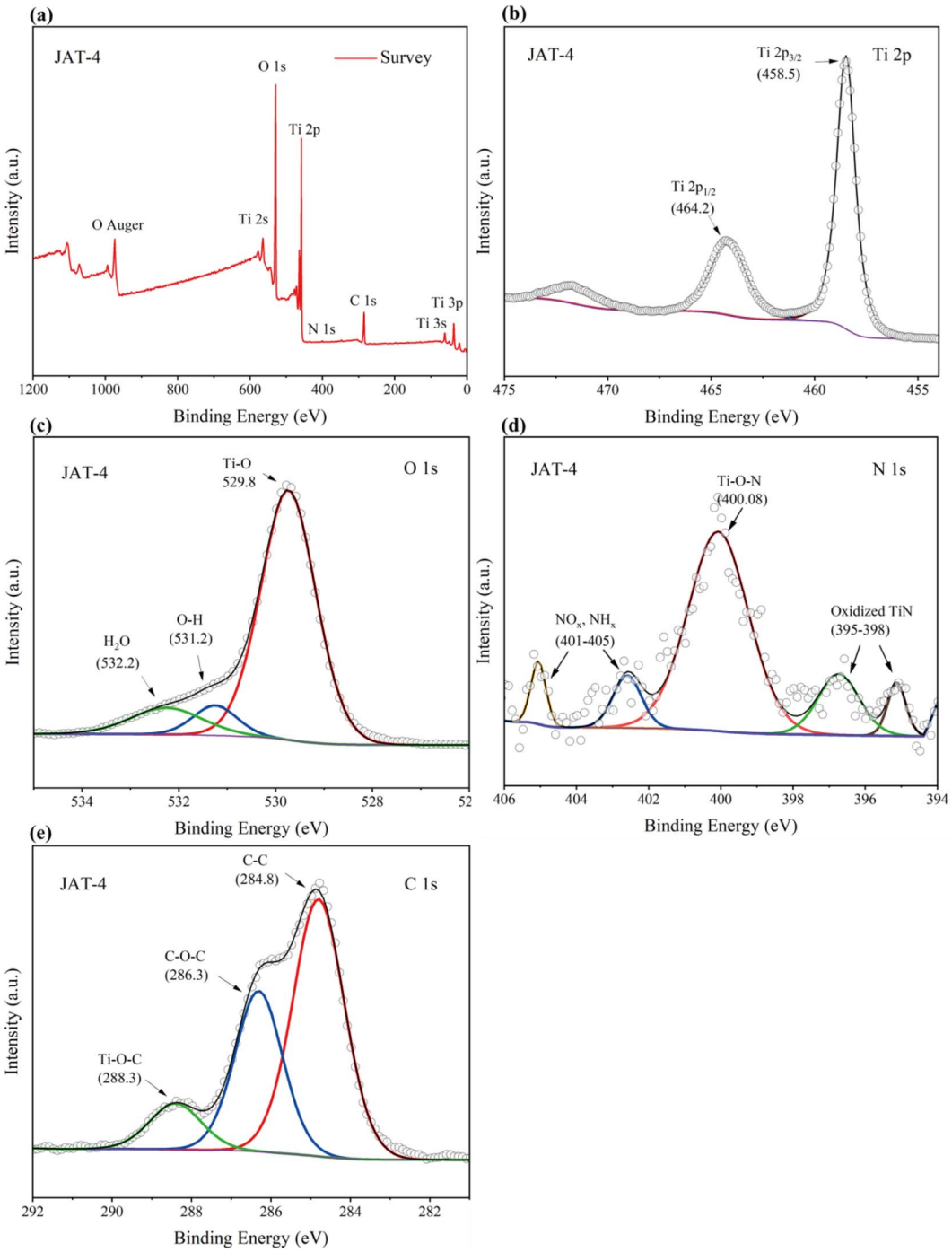

Fig. 7 Fully scanned XPS spectrum (a) of JAT-4 nanocrystals, XPS spectra of Ti 2p (b), XPS spectra of O1s (c), XPS spectra of N 1s (d) and XPS spectra of C1s (e) for the JAT-4 nanocrystals.

3.3 Analysis of the photoelectric performance of the photocatalysts

The UV-vis diffuse reflectance spectra of the JAT and JNT nanocrystals are exhibited in Fig. 9a and b. They were found to have a broad background absorption in the visible light region compared to the pure TiO_2. On the one hand, this can be associated with the doping of nitrogen in N–TiO_2/C nanocrystals, which were capable of narrowing the band gap to shift the light absorption to the visible region.[3,9,41–47] On the other hand, the carbon modifying the surface of N–TiO_2/C could also absorb visible light and reduce the reflection of light, resulting in their absorption edge shifting to the visible light range according to previous reports.[22,47–53] The significant red shifts also matched with the light brown-yellow color of JAT and JNT powders. It was obvious that the visible light absorption

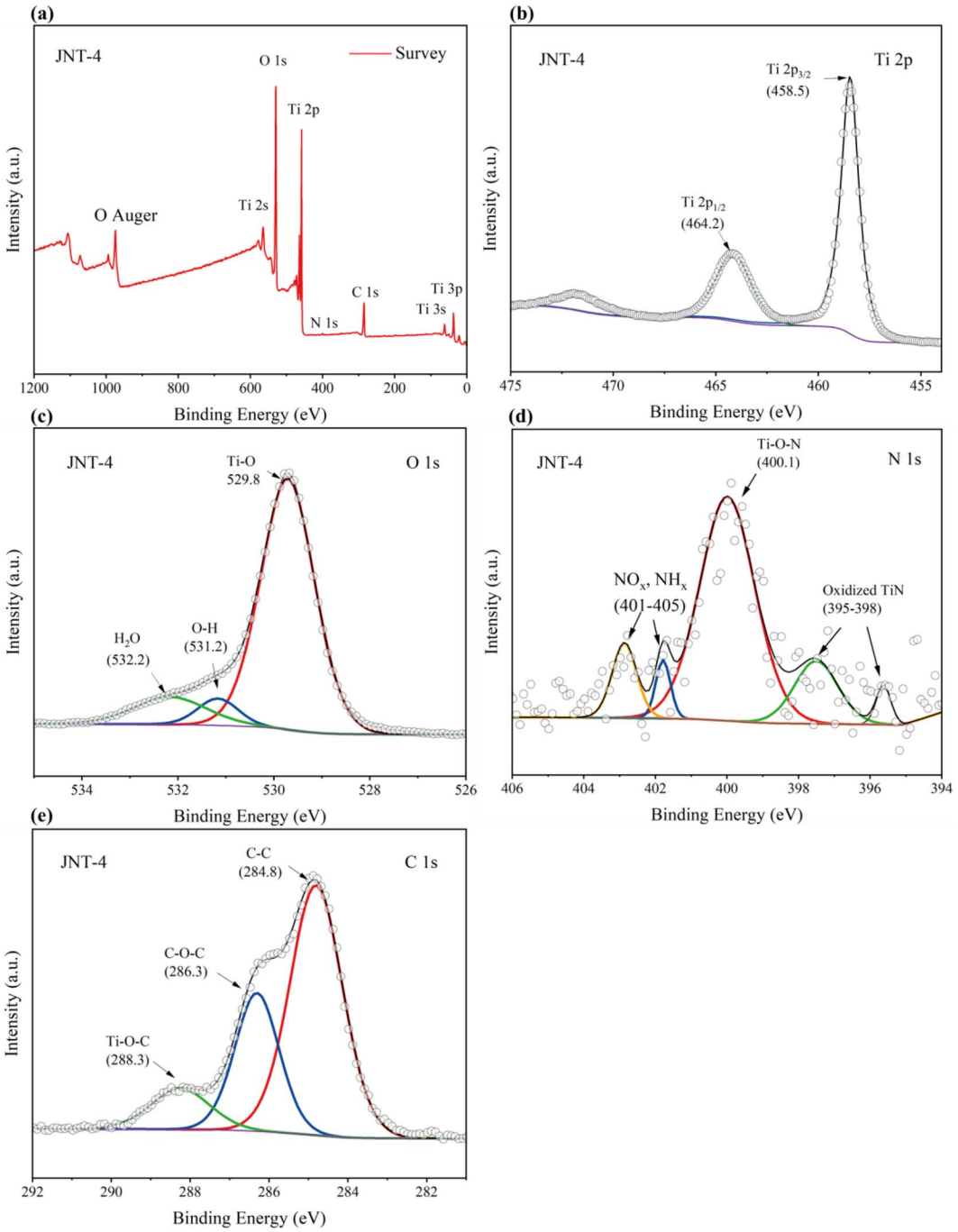

Fig. 8 Fully scanned XPS spectrum (a) of JNT-4 nanocrystals, XPS spectra of Ti 2p (b), XPS spectra of O1s (c), XPS spectra of N 1 s (d) and XPS spectra of C1s (e) for the JNT-4 nanocrystals.

ability of JNT nanocrystals was better than that of JAT nanocrystals at the same volume ratio of jellyfish mucus added to tetrabutyl titanate (TBT). The JNT-4 nanocrystal exhibited the strongest visible light absorption from 400 nm to 700 nm.

The optical band gap energies of JAT-4 and JNT-4 nanocrystals were also estimated from Fig. 9c and d based on the Kubelka–Munk function.[54] The linear equations were fitted in the medium linear section of the plots, where the intercepts on the *x*-axis showed that the band gap energy of pure TiO_2 was 3.20 eV. However, those of JAT-4 and JNT-4 nanocrystals were 2.95 eV and 2.91 eV, respectively. Therefore, the conduction band and valence band of JAT-4 and JNT-4 nanocrystals were more negative than those of pure TiO_2. It suggested that these N–TiO_2/C nanocrystals had visible light photocatalytic activity and their electrons could migrate from the valence band to the conduction band upon absorbing visible light. Compared to the

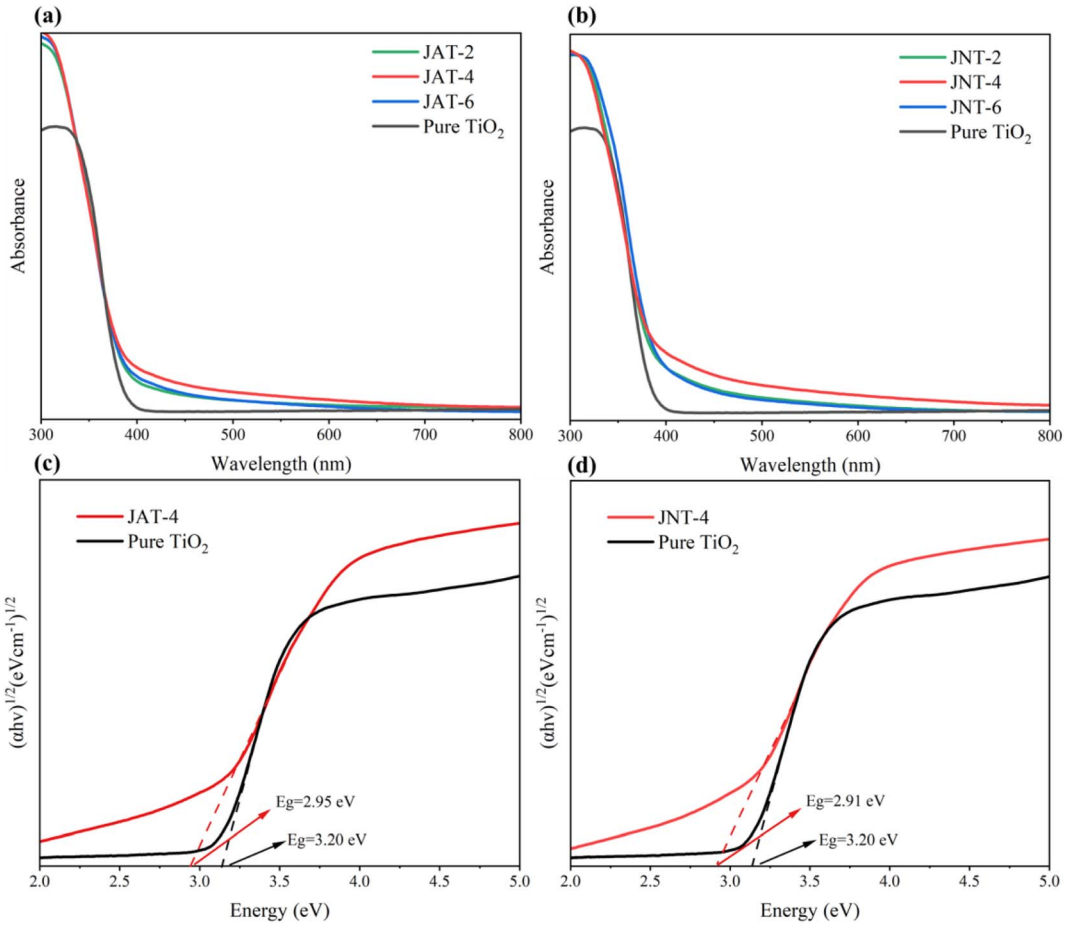

Fig. 9 UV-vis absorption spectra (a and b) of JAT and JNT nanocrystals and the corresponding band gap energy (E_g) (c and d) of JAT-4 and JNT-4 nanocrystals.

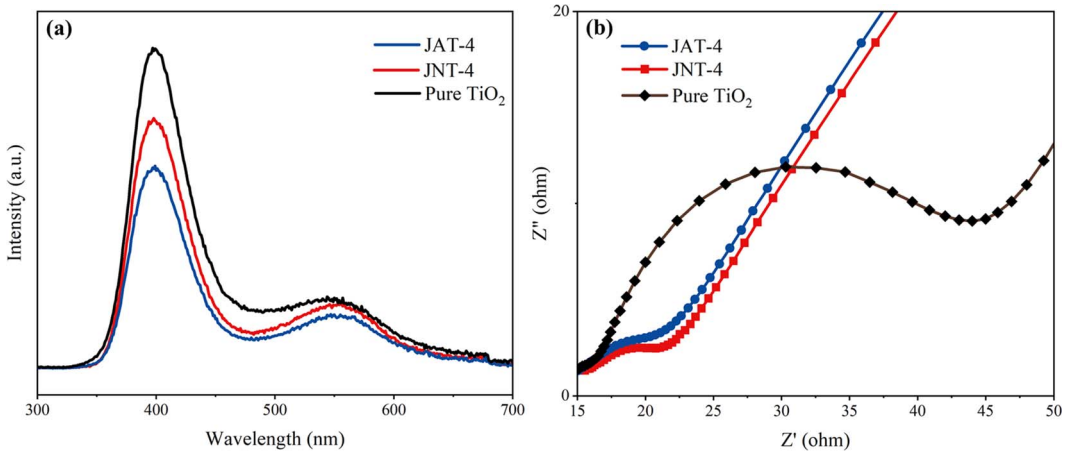

Fig. 10 PL spectrum (a) and Nyquist plot (b) of JAT-4, JNT-4 nanocrystals and pure TiO_2.

JAT-4 nanocrystal, the separation of photogenerated electron–hole pairs under visible light irradiation may be more feasible for the JNT-4 nanocrystal owing to its lower band gap energy based on previous reports.[16,37]

The photoluminescence performance of JAT-4 and JNT-4 nanocrystals was evaluated from the PL spectrum. Both N–TiO_2/C nanocrystals have lower PL spectral peak intensity than pure TiO_2 (Fig. 10a). It can be concluded that the N doping and C modification in JAT and JNT nanocrystals may suppress the

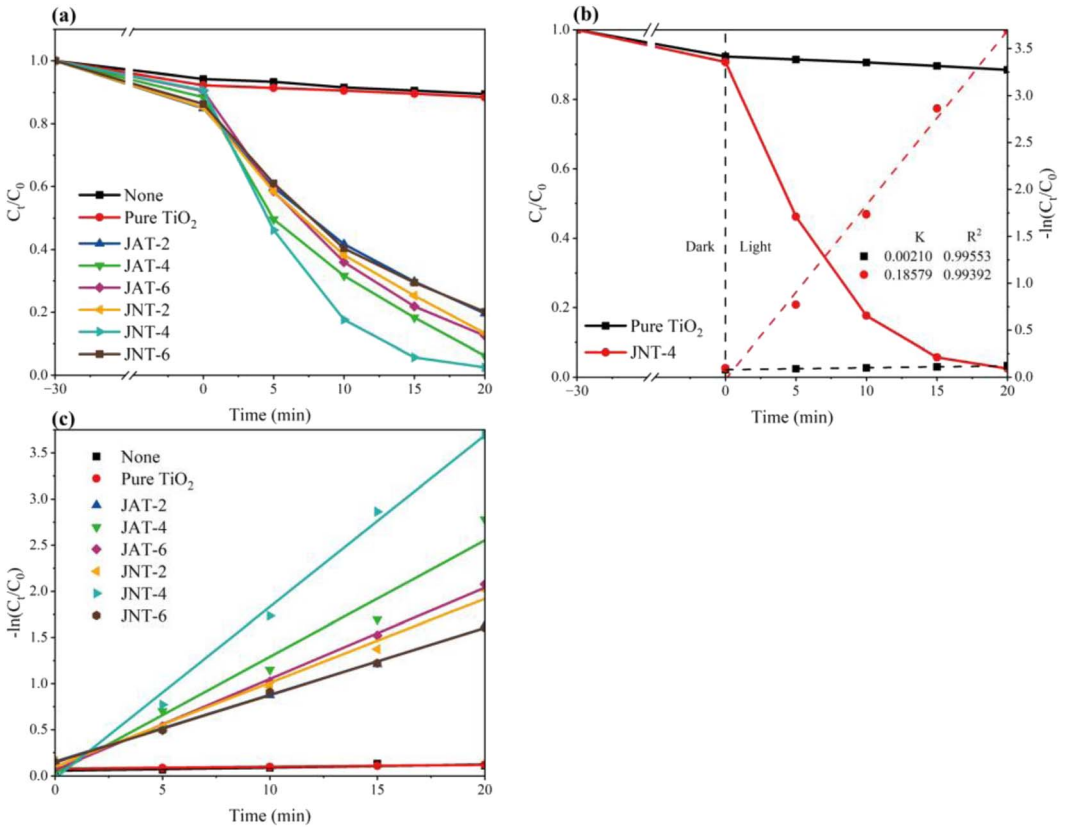

Fig. 11 Photocatalytic degradation (a) and the corresponding $-\ln(C_t/C_0)$ variations (b and c) of RhB with JAT, JNT nanocrystals, pure TiO_2 and without photocatalysts under a mercury lamp ($\lambda \geq 400$ nm).

recombination of electron–hole pairs and promote the separation of photogenerated charge carriers, thus resulting in the improvement of their photocatalytic capability. EIS was used to reflect the separation efficiency of photogenerated charge carriers. The radius of the impedance arc in the Nyquist plot represents the negative correlation with charge transfer and separation efficiency, which significantly reduced for JAT-4 and JNT-4 nanocrystals compared to pure TiO_2 as shown in Fig. 10b. It indicated that these modified nanocrystals had lower electron transfer resistance, which was beneficial for the transfer and separation of photogenerated electron–hole pairs. Thus, they showed good photocatalytic performance. The result also suggested that the JNT-4 nanocrystal might show a more effective separation of photogenerated electron–hole pairs and faster interfacial electron transfer compared to the JAT-4 nanocrystal due to the smaller radius of its impedance arc.

3.4 Photocatalytic degradation of RhB

The photocatalytic degradation of RhB was measured to examine the photodegradation abilities of the JAT and JNT nanocrystals. According to the relationships between the concentration ratio (C_t/C_0) and time for RhB degradation in Fig. 11a, only 11.54% of RhB was degraded by pure TiO_2, but the JAT and JNT nanocrystals exhibited excellent visible-light photocatalytic activities for RhB degradation. Their photocatalytic degradation efficiency first increased and then decreased along with the increase in the volume ratio between their mucus proteins utilized and TBT. The JNT-4 nanocrystal had the highest photocatalytic activity among the 6 N–TiO_2/C nanocrystals, and the concentration of RhB decreased by 97.52% (Fig. 11a). Thus, the visible-light photocatalytic activity was obviously improved in the JNT-4 nanocrystal compared to some other doped TiO_2 nanocrystals.[40,55–58]

The kinetics of the photocatalytic reduction of RhB is described in Fig. 11b and c. The first order rate constant k (min^{-1}) of 6 N–TiO_2/C nanocrystals was calculated from the first order equation $\ln(C_0/C_t) = -kt$. The k value was only 0.00210 min^{-1} for pure TiO_2, but reached 0.18579 min^{-1} for the JNT-4 nanocrystal. These results indicated that jellyfish mucus proteins could regulate the functional properties of TiO_2. The highest photocatalytic activity may be attributed to the optimal balance of mesoporous structures, C, N content and amount of residual proteins, as previously reported for the doped TiO_2 nanocrystals derived from the extrapallial fluid of live mussels.[26] While the ratio of jellyfish mucus proteins to TBT reached 6 : 1, the reduction in crystallinity and the presence of residual proteins may result in low photocatalytic activity. At the protein

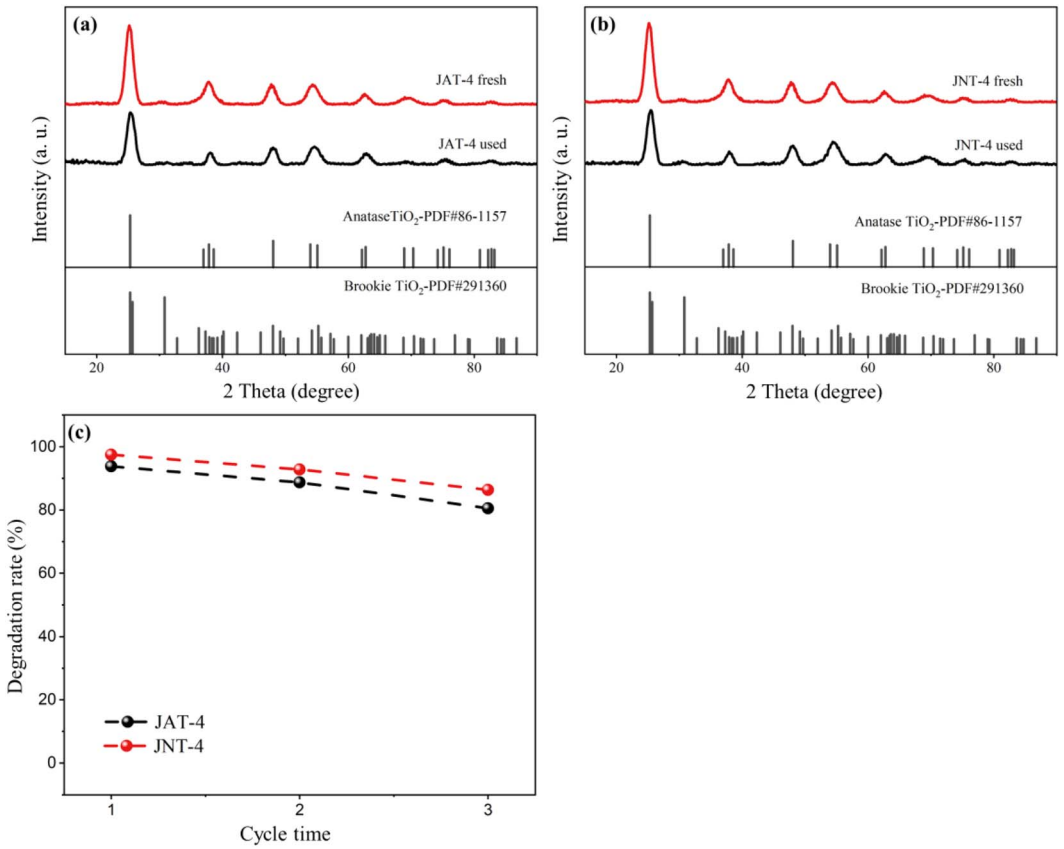

Fig. 12 X-ray diffraction patterns of JAT-4 and JNT-4 nanocrystals before and after the photocatalytic degradation experiment (a and b), and recycling tests of photocatalytic degradation of RhB using JAT-4 and JNT-4 nanocrystals (c).

to TBT ratio of 4 : 1, JNT-4 nanocrystals showed higher photocatalytic activity than JAT-4 nanocrystals, which may be due to the difference in mesoporous structures caused by the two jellyfish mucus. The XRD spectra of both nanocrystals before and after photocatalytic degradation showed that there was no significant change in the crystal structure even through multiple degradation reactions (Fig. 12a and b). During three photodegradation cycles of RhB for the JAT-4 and JNT-4 nanocrystals (Fig. 12c), the photocatalytic activity did not exhibit any significant loss. It implied that these N–TiO_2/C nanocrystals were relatively stable and did not corrode during the photocatalytic oxidation of pollutant molecules.

3.5 Free radical analysis in the photocatalytic process

The main active species in the degradation of organic pollutants by the synthesized N–TiO_2/C nanocrystals from jellyfish mucus were tested by electron spin resonance (ESR) and scavenger experiments referring to previous studies.[16,37,59] As shown in Fig. 13, four active species including superoxide radicals ($^{\bullet}O_2^-$), singlet oxygen ($^1O_2$), photogenerated holes (h^+) and hydroxyl radicals ($^{\bullet}OH$) were detected. $^{\bullet}O_2^-$, h^+ and $^{\bullet}OH$ were found to have obvious characteristic peaks. *p*-Benzoquinone (BQ), L-histidine, ethylene diamine tetraacetic acid (EDTA), and isopropanol (IPA) were used as the scavengers for $^{\bullet}O_2^-$, $^1O_2$, h^+ and $^{\bullet}OH$, respectively. For the JNT-4 nanocrystal, the degradation rate of RhB reached 97.52% without the scavengers (Fig. 11a). However, it decreased to 21.07%, 84.58%, 37.27% and 27.14%, respectively, when BQ, L-histidine, EDTA, and IPA scavengers were added (Fig. 14). The results indicated that $^{\bullet}O_2^-$, h^+ and $^{\bullet}OH$ played a dominant role in the degradation process of RhB.

3.6 Analysis of the photocatalytic degradation mechanism under visible light

The XPS valence band spectrum showed that the JNT-4 nanocrystal had a valence band of 2.41 eV (Fig. S6†). Its electronic band structure was calculated in combination with the band gap of 2.91 eV. The visible light photocatalytic mechanism was thus inferred from Fig. 15. It has been widely reported that N doping in the TiO_2 lattice would promote the formation of new mid-gap energy states of N 2p orbitals above the O 2p valence band, which could narrow the band gap and shift the optical absorption to the visible light region.[3,9,41–46] Besides, under visible light irradiation, the carbon on the surface was capable of increasing the visible light absorption and decreasing the light reflection as a sensitizer.[22,26] The carbon modified on the surface could also develop the carbonaceous layer, which

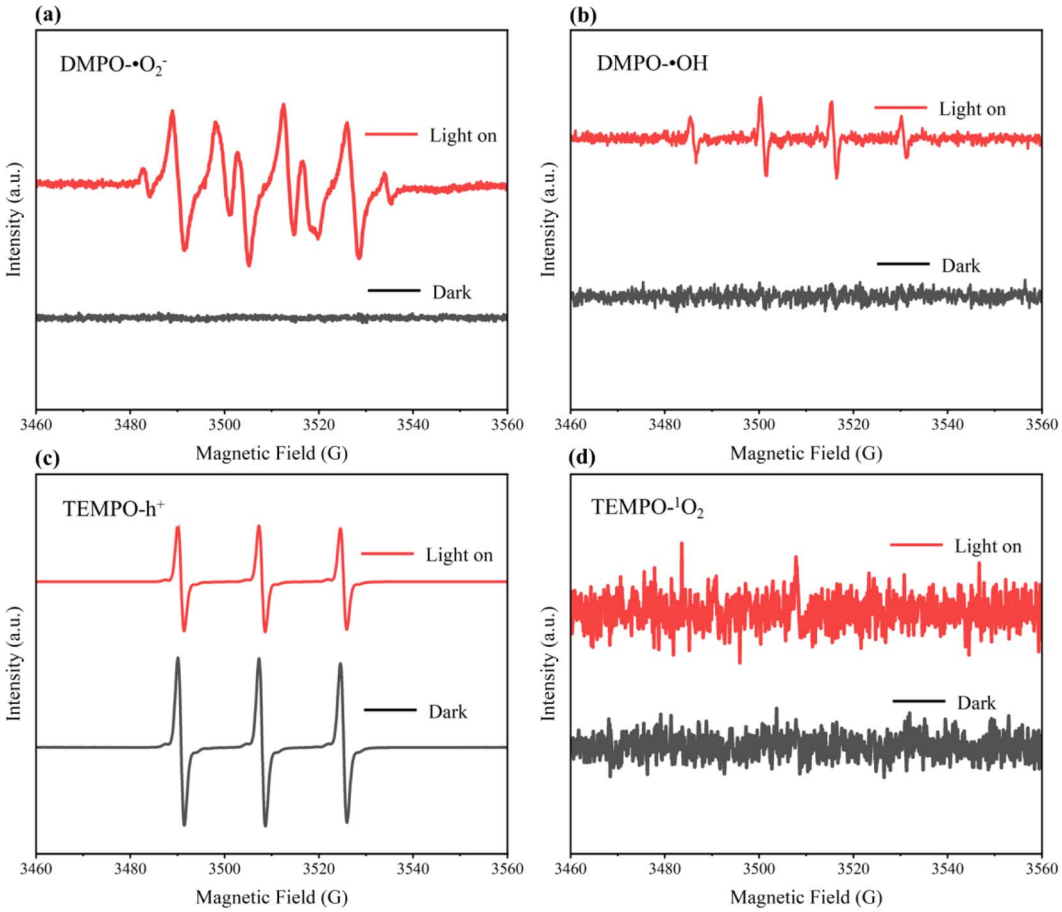

Fig. 13 ESR spectra of DMPO-$^{\bullet}O_2^-$ (a), DMPO-$^{\bullet}$OH (b), TEMPO-h^+ (c) and TEMPO-$^1O_2$ (d) of JNT-4 nanocrystals in the dark and under mercury lamp ($\lambda \geq 400$ nm) irradiation.

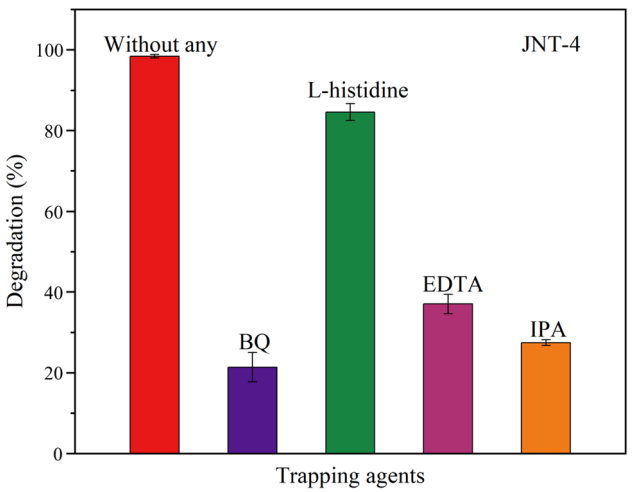

Fig. 14 Photocatalytic degradation efficiency of RhB for JNT-4 nanocrystals in the presence of different scavengers under mercury lamp ($\lambda \geq 400$ nm) irradiation.

contributed to the separation of the photogenerated electron–hole pairs and maintained high reactivity.[22,50]

During the photocatalytic degradation of RhB, the JNT-4 nanocrystal was thus activated when the visible light was irradiated. The photogenerated electrons (e^-) and holes (h^+) were formed (eqn (2)). The e^- easily migrated to the conduction band, and the h^+ were produced in the valence band. Because the redox potential of the conduction band position was higher than that of $O_2/^{\bullet}O_2^-$ (−0.33 eV *vs.* normal hydrogen electrode (NHE)),[60] and the level of valence band was lower than those of $H_2O/^{\bullet}OH$ (2.27 eV *vs.* normal hydrogen electrode (NHE)) and $^{\bullet}O_2^-/^1O_2$ (0.34 eV *vs.* NHE),[61] the h^+ could oxidize water in the reaction system to produce $^{\bullet}OH$ (eqn (3)) and the e^- could trap the O_2 to generate a large number of $^{\bullet}O_2^-$ (eqn (4)). The $^1O_2$ was then produced from the further reaction of h^+ and $^{\bullet}O_2^-$ (eqn (5)). RhB was thus gradually photodegraded by the combined action of the four active species (eqn (6) and (7)). It can be seen that the synergistic heterostructure of N–TiO_2/C nanocrystals synthesized by jellyfish mucus not only acts as an electron collector and transporter to inhibit the recombination of electron–hole pairs, but also provides easy access to the active charge transfer transitions under visible light for the efficient degradation of organic pollutants.

$$\text{Photocatalyst} + hv \rightarrow h^+ + e^- \quad (2)$$

$$h^+ + H_2O \rightarrow {}^{\bullet}OH \quad (3)$$

$$e^- + O_2 \rightarrow {}^{\bullet}O_2^- \quad (4)$$

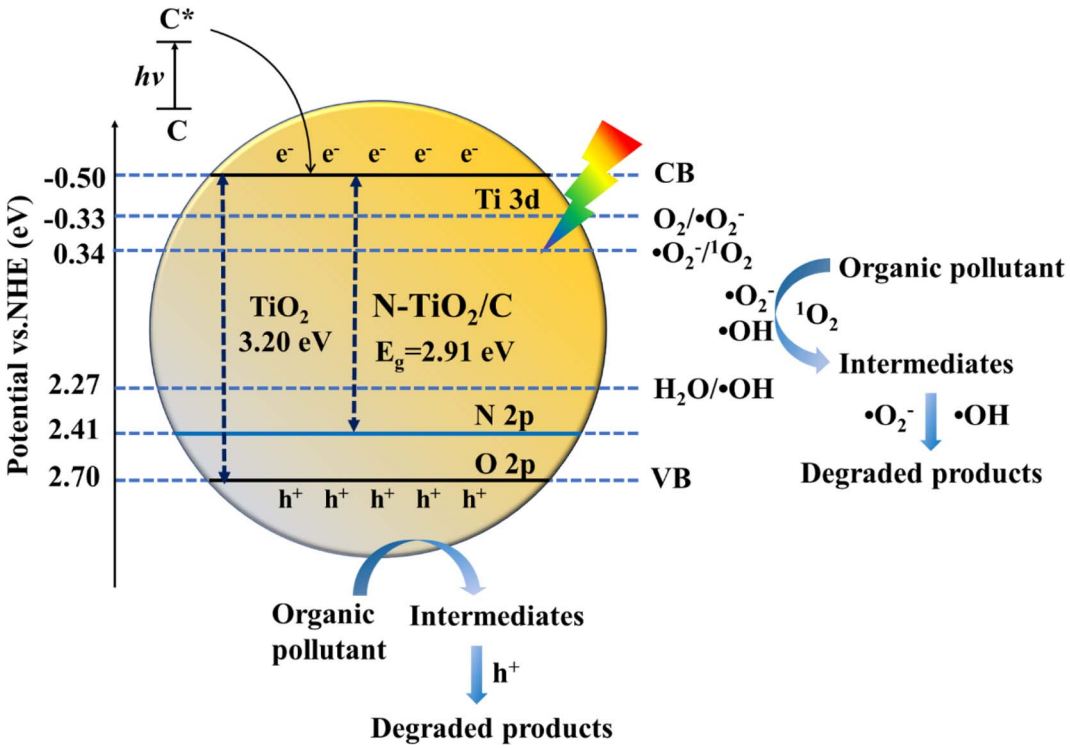

Fig. 15 Schematic illustration of the proposed visible photocatalytic mechanism of organic pollutants using JNT-4 nanocrystals.

$$h^+ + {}^{\bullet}O_2^- \rightarrow {}^1O_2 \quad (5)$$

$$h^+ + \text{Photocatalyst} \rightarrow \text{Intermediates} \rightarrow \text{Degraded products} \quad (6)$$

$$^{\bullet}OH/^{\bullet}O_2^-/{}^1O_2 + \text{Photocatalyst} \rightarrow \text{Intermediates} \rightarrow \text{Degraded products} \quad (7)$$

4 Conclusions

Mesoporous N–TiO_2/C nanocrystals were successfully fabricated by utilizing the mucus proteins of large harmful jellyfish *A. coerulea* and *N. nomurai*, which had frequently bloomed in East Asian marginal seas in recent decades, as natural doping sources in this study. This bio-inspired synthesis was developed at a low temperature by a simple "one-pot" hydrothermal method. The prepared N–TiO_2/C nanocrystals were identified as a mixed phase structure composed of the dominant anatase phase and a small amount of brookite phase TiO_2, where the four elements Ti, O, N, and C were uniformly distributed throughout the entire materials. The mesoporous structures including surface area, pore size and pore volume varied with the change in the volume ratio of jellyfish mucus to TBT. The surface area and pore volume of N–TiO_2/C nanocrystals from *N. nomurai* were larger than those from *A. coerulea* at the same volume ratio, but the pore size became smaller. The N doping and C modification in these nanocrystals could narrow the band gap, promote the separation of photogenerated charge carriers and the absorption of visible light, thus resulting in the improvement of visible light photocatalytic activity. The photocatalytic degradation efficiency of RhB first increased and then decreased with the increase in the volume ratio of jellyfish mucus proteins to TBT under the visible light irradiation. The highest photocatalytic activity was observed in the N–TiO_2/C nanocrystal from *N. nomurai* at the volume ratio of 4 : 1, which exhibited the strongest visible light absorption, lower band gap energy and smaller electron transfer resistance. The synthesized N–TiO_2/C nanocrystals have a relatively stable crystal structure even through multiple degradation reactions. The ESR spectroscopy and scavenger experiments revealed that the main active species including $^{\bullet}O_2^-$, h^+ and $^{\bullet}OH$ played major roles in the degradation process of RhB. Therefore, this study not only provides a new insight into the synthesis of N-doped TiO_2 with C modification by a simple and economical method, but also a new approach for the high value re-utilization of harmful jellyfish *A. coerulea* and *N. nomurai* in the East Asian marginal seas. The N–TiO_2/C nanocrystals synthesized using their mucus showed high visible-light photocatalytic efficiency under the influence of a synergistic heterostructure.

Data availability

Data will be made available on request.

Author contributions

Song Feng: investigation, formal analysis, writing-original draft, project administration, funding acquisition. Lingchen Liu:

investigation, data curation, formal analysis, visualization. Jianing Lin: conceptualization, visualization, project administration, writing-review & editing. Ziwei Wang: methodology, formal analysis, visualization. Jinzeng Gu: investigation, software. Lutao Zhang: investigation, software. Bin Zhang: project administration, funding acquisition. Song Sun: project administration, funding acquisition.

Conflicts of interest

The authors declare that they have no known competing financial interests or personal relationships that could have appeared to influence the work reported in this paper.

Acknowledgements

We are grateful to Fisherman Guangshui Yu for helping to collect the *N. nomurai* mucus. This research was supported by the National Key Research and Development Program of China (grant no. 2023YFC3108204), National Natural Science Foundation of China (grant no. 42176136, 42211540390 and 42130411), "Future Partner Network" Project of the Chinese Academy of Sciences (grant no. 058GJHZ2022097FN), the Natural Science Foundation of Shandong Province (grant no. ZR2020KE047), the Ministry of Education Chun Hui plan project (grant no. 202201136), Youth Innovation Promotion Association Project, Chinese Academy of Sciences and Huiquan Scholar, Institute of Oceanology, Chinese Academy of Sciences to Song Feng.

References

1 M. C. Ariza-Tarazona, J. F. Villarreal-Chiu, J. M. Hernández-López, J. R. De la Rosa, V. Barbieri, C. Siligardi and E. I. Cedillo-González, Microplastic pollution reduction by a carbon and nitrogen-doped TiO_2: Effect of pH and temperature in the photocatalytic degradation process, *J. Hazard. Mater.*, 2020, **395**, 122632.

2 W. Zhong, B. Shan, W. Tan and S. Luo, Advances on photocatalytic treatment of microplastics in water, *Fine Chem.*, 2023, **40**, 1176–1186.

3 R. Asahi, T. Morikawa, T. Ohwaki, K. Aoki and Y. Taga, Visible-light photocatalysis in nitrogen-doped titanium oxides, *Science*, 2001, **293**, 269–271.

4 R. Li, T. Gao, Y. Wang, Y. Chen, W. Luo, Y. Wu, Y. Xie, Y. Wang and Y. Zhang, Engineering of bimetallic Au-Pd alloyed particles on nitrogen defects riched g-C_3N_4 for efficient photocatalytic hydrogen production, *Int. J. Hydrogen Energy*, 2024, **63**, 1116–1127.

5 W. Tang, H. Ye, Y. Xie, P. Chen, L. Luo and Y. Zhang, Transition metal bismuth spheres dispersed and anchored in benzene-ring-grafted porous g-C_3N_4 nanosheets for photocatalytic reduction of CO_2, *Chem. Eng. J.*, 2023, **478**, 147350.

6 Y. Wang, T. Gao, R. Li, Y. Chen, W. Luo, Y. Wu, Y. Xie, Y. Wang and Y. Zhang, Layered deposited MoS_2 nanosheets on acorn leaf like CdS as an efficient anti-photocorrosion photocatalyst for hydrogen production, *Fuel*, 2024, **368**, 131621.

7 Y. Wang, L. Liu, T. Ma, Y. Zhang and H. Huang, 2D Graphitic carbon nitride for energy conversion and storage, *Adv. Funct. Mater.*, 2021, **31**, 2102540.

8 L. Zhao, *Simultaneous Synthesis, Photocatalytic Activity and Characterization of Biomass Multi-Elements Co-doped TiO_2*, Doctoral Thesis, Huaqiao University, 2019, pp. 1–118.

9 J. Wang, D. N. Tafen, J. P. Lewis, Z. Hong, A. Manivannan, M. Zhi, M. Li and N. Wu, Origin of photocatalytic activity of nitrogen-doped TiO_2 nanobelts, *J. Am. Chem. Soc.*, 2009, **131**, 12290–12297.

10 N. Wei, H. Cui, Q. Song, L. Zhang, X. Song, Y. Wang, Y. Zhang, J. Li, J. Wen and J. Tian, Ag_2O nanoparticle/TiO_2 nanobelt heterostructures with remarkable photo-response and photocatalytic properties under UV, visible and near-infrared irradiation, *Appl. Catal., B*, 2016, **198**, 83–90.

11 Y. Zhang, Z. Zhao, J. Chen, L. Cheng, J. Chang, W. Sheng, C. Hu and S. Cao, C-doped hollow TiO_2 spheres: in situ synthesis, controlled shell thickness, and superior visible-light photocatalytic activity, *Appl. Catal., B*, 2015, **165**, 715–722.

12 D. Vernardou, H. Drosos, E. Spanakis, E. Koudoumas, C. Savvakis and N. Katsarakis, Electrochemical and photocatalytic properties of WO_3 coatings grown at low temperatures, *J. Mater. Chem.*, 2011, **21**, 513–517.

13 A. Naldoni, M. Allieta, S. Santangelo, M. Marelli, F. Fabbri, S. Cappelli, C. L. Bianchi, R. Psaro and V. Dal Santo, Effect of nature and location of defects on bandgap narrowing in black TiO_2 nanoparticles, *J. Am. Chem. Soc.*, 2012, **134**, 7600–7603.

14 F. Dong, S. Guo, H. Wang, X. Li and Z. Wu, Enhancement of the visible light photocatalytic activity of C-doped TiO_2 nanomaterials prepared by a green synthetic approach, *J. Phys. Chem. C*, 2011, **115**, 13285–13292.

15 C. Xue, T. Wang, G. Yang, B. Yang and S. Ding, A facile strategy for the synthesis of hierarchical TiO_2/CdS hollow sphere heterostructures with excellent visible light activity, *J. Mater. Chem. A*, 2014, **2**, 7674–7679.

16 Z. Lu, L. Zeng, W. Song, Z. Qin, D. Zeng and C. Xie, In situ synthesis of C-TiO_2/g-C_3N_4 heterojunction nanocomposite as highly visible light active photocatalyst originated from effective interfacial charge transfer, *Appl. Catal., B*, 2017, **202**, 489–499.

17 J. Chen, F. Qiu, W. Xu, S. Cao and H. Zhu, Recent progress in enhancing photocatalytic efficiency of TiO2-based materials, *Appl. Catal., A*, 2015, **495**, 131–140.

18 L. Jing, W. Zhou, G. Tian and H. Fu, Surface tuning for oxide-based nanomaterials as efficient photocatalysts, *Chem. Soc. Rev.*, 2013, **42**, 9509–9549.

19 J. Li, L. Gao and W. Gan, Bioinspired C/TiO_2 photocatalyst for rhodamine B degradation under visible light irradiation, *Front. Agr. Sci. Eng.*, 2017, **4**, 459–464.

20 J. Shao, W. Sheng, M. Wang, S. Li, J. Chen, Y. Zhang and S. Cao, In situ synthesis of carbon-doped TiO_2 single-crystal nanorods with a remarkably photocatalytic efficiency, *Appl. Catal., B*, 2017, **209**, 311–319.

21 R. Purbia, R. Borah and S. Paria, Carbon-doped mesoporous anatase TiO_2 multi-tubes nanostructures for highly improved visible light photocatalytic activity, *Inorg. Chem.*, 2017, **56**, 10107–10116.

22 L. Zhao, X. Chen, X. Wang, Y. Zhang, W. Wei, Y. Sun, M. Antonietti and M. Titirici, One-step solvothermal synthesis of a carbon@TiO_2 dyade structure effectively promoting visible-light photocatalysis, *Adv. Mater.*, 2010, **22**, 3317–3321.

23 A. Piatkowska, M. Janus, K. Szymanski and S. Mozia, C-, N- and S-Doped TiO_2 Photocatalysts: A Review, *Catalysts*, 2011, **11**, 144.

24 D. Wang, J. Li, X. Wu, L. Lu and A. Xu, One-step hydrothermal synthesis of N-doped TiO_2/C nanocomposites with high visible light photocatalytic activity, *Nanoscale*, 2012, **4**, 576–584.

25 M. Ilyas, A. Waris, A. U. Khan, D. Zamel, L. Yar, A. Baset, A. Muhaymin, S. Khan, A. Ali and A. Ahmad, Biological synthesis of titanium dioxide nanoparticles from plants and microorganisms and their potential biomedical applications, *Inorg. Chem. Commun.*, 2021, **133**, 108968.

26 H. Zeng, J. Xie, H. Xie, B. L. Su, M. Wang, H. Ping, W. Wang, H. Wang and Z. Fu, Bioprocess-inspired synthesis of hierarchically porous nitrogen-doped TiO_2 with high visible-light photocatalytic activity, *J. Mater. Chem. A*, 2015, **3**, 19588–19596.

27 C. Duarte, K. A. Pitt and C. H. Lucas, Introduction: understanding jellyfish blooms, In *Jellyfish Blooms*, ed. C. H. Lucas and K. A. Pitt, Springer, Dordrecht, 2014, pp. 1–5.

28 J. E. Purcell, S. I. Uye and W. T. Lo, Anthropogenic causes of jellyfish blooms and their direct consequences for humans: a review, *Mar. Ecol.: Prog. Ser.*, 2007, **350**, 153–174.

29 A. J. Richardson, A. Bakun, G. C. Hays and M. J. Gibbons, The jellyfish joyride: causes, consequences and management responses to a more gelatinous future, *Trends Ecol. Evol.*, 2009, **24**, 312–322.

30 S. Feng, S. Sun, C. Li and F. Zhang, Controls of *Aurelia coerulea* and *Nemopilema nomurai* (Cnidaria: Scyphozoa) blooms in the coastal sea of China: strategies and measures, *Front. Mar. Sci.*, 2022, **9**, 946830.

31 D. Patel and M. Brinchmann, Skin mucus proteins of lumpsucker (*Cyclopterus lumpus*), *Biochem. Biophys. Rep.*, 2017, **9**, 217–225.

32 A. Patwa, A. Thiéry, F. Lombard, M. Lilley, C. Boisset, J. Bramard, J. Bottero and P. Barthélémy, Accumulation of nanoparticles in "jellyfish" mucus: a bio-inspired route to decontamination of nano-waste, *Sci. Rep.*, 2015, **5**, 11387.

33 R. Li, H. Yu, R. Xing, S. Liu, Y. Qing, K. Li, B. Li, X. Meng, J. Cui and P. Li, Application of nanoLC-MS/MS to the shotgun proteomic analysis of the nematocyst proteins from jellyfish *Stomolophus meleagris*, *J. Chromatogr. B*, 2012, **899**, 86–95.

34 W. Liu, F. Mo, G. Jiang, H. Liang, C. Ma, T. Li, L. Zhang, L. Xiong, G. Mariottini, J. Zhang and L. Xiao, Stress-induced mucus secretion and its composition by a combination of proteomics and metabolomics of the jellyfish *Aurelia coerulea*, *Mar. Drugs*, 2018, **16**, 341.

35 D. Zhou, *Preparation of TiO_2-Based-Photocatalytic Materials and Degradation Performance of Pet Fiber-Based Microplastics*, Master Dissertation, Donghua University, 2021, pp. 1–98.

36 X. Liu, Y. Chen, C. Cao, J. Xu, Q. Qian, Y. Luo, H. Xue, L. Xiao, Y. Chen and Q. Chen, Electrospun nitrogen and carbon co-doped porous TiO_2 nanofibers with high visible light photocatalytic activity, *New J. Chem.*, 2015, **39**, 6944.

37 G. Zhu, X. Yang, Y. Liu, Y. Zeng, T. Wang and H. Yu, One-pot synthesis of C-modified and N-doped TiO_2 for enhanced visible-light photocatalytic activity, *J. Alloys Compd.*, 2022, **902**, 163677.

38 J. Pan, X. Zhang, A. Du, D. Sun and J. Leckie, Self-etching reconstruction of hierarchically mesoporous F-TiO_2 hollow microspherical photocatalyst for concurrent membrane water purifications, *J. Am. Chem. Soc.*, 2008, **130**, 11256–11257.

39 T. Jia, F. Fu, D. Yu, J. Cao and G. Sun, Facile synthesis and characterization of N-doped TiO_2/C nanocomposites with enhanced visible light photocatalytic performance, *Appl. Surf. Sci.*, 2014, **430**, 438–447.

40 T. Wang, X. Yan, S. Zhao, B. Lin, C. Xue, G. Yang, S. Ding, B. Yang, C. Ma, G. Yang and G. Yang, A facile one-step synthesis of three-dimensionally ordered macroporous N-doped TiO_2 with ethanediamine as the nitrogen source, *J. Mater. Chem. A*, 2014, **2**, 15611–15619.

41 X. Chen, L. Liu, P. Yu and S. Mao, Increasing solar absorption for photocatalysis with black hydrogenated titanium dioxide nanocrystals, *Science*, 2011, **331**, 746–750.

42 D. Mitoraj and H. Kisch, The nature of nitrogen-modified titanium dioxide photocatalysts active in visible light, *Angew. Chem., Int. Ed.*, 2008, **47**, 9975–9978.

43 M. Xing, J. Zhang and F. Chen, New approaches to prepare nitrogen-doped TiO_2 photocatalysts and study on their photocatalytic activities in visible light, *Appl. Catal., B*, 2009, **89**, 563–569.

44 V. Etacheri, M. Seery, S. Hinder and S. Pillai, Highly visible light active TiO_2-xNx heterojunction photocatalysts, *Chem. Mater.*, 2010, **22**, 3843–3853.

45 M. Sathish, B. Viswanathan, R. P. Viswanath and C. S. Gopinath, Synthesis, characterization, electronic structure, and photocatalytic activity of nitrogen-doped TiO_2 nanocatalyst, *Chem. Mater.*, 2005, **17**, 6349–6353.

46 S. Yin, Y. Aita, M. Komatsu, J. S. Wang, Q. Tang and T. Sato, Synthesis of excellent visible-light responsive TiO_2-xNy photocatalyst by a homogeneous precipitation-solvothermal process, *J. Mater. Chem.*, 2005, **15**, 674–682.

47 P. Zabek, J. Eberl and H. Kisch, On the origin of visible light activity in carbon-modified titania, *Photochem. Photobiol. Sci.*, 2009, **8**, 264–269.

48 C. Chen, W. Cai, M. Long, B. Zhou, Y. Wu, D. Wu and Y. Feng, Synthesis of visible-light responsive graphene oxide/TiO_2 composites with p/n heterojunction, *ACS Nano*, 2010, **4**, 6425–6432.

49 H. Liu, Y. Wu and J. Zhang, A new approach toward carbon-modified vanadium-doped titanium dioxide photocatalysts, *ACS Appl. Mater. Interfaces*, 2011, **3**, 1757–1764.

50 F. Jia, Z. Yao, Z. Jiang and C. Li, Preparation of carbon coated TiO_2 nanotubes film and its catalytic application for H_2 generation, *Catal. Commun.*, 2011, **12**, 497–501.
51 X. Zhang, H. Li, X. Cui and Y. Lin, Graphene/TiO_2 nanocomposites: synthesis, characterization and application in hydrogen evolution from water photocatalytic splitting, *J. Mater. Chem.*, 2010, **20**, 2801–2806.
52 L. Jia, D. Wang, Y. Huang, A. Xu and H. Yu, Highly durable N-doped graphene/CdS nanocomposites with enhanced photocatalytic hydrogen evolution from water under visible light irradiation, *J. Phys. Chem. C*, 2011, **115**, 11466–11473.
53 H. Zhang, X. Lv, Y. Li, Y. Wang and J. Li, P25-Graphene composite as a high performance photocatalyst, *ACS Nano*, 2010, **4**, 380–386.
54 H. Qian, Q. Hou, E. Duan, J. Niu, Y. Nie, C. Bai, X. Bai and M. Ju, Honeycombed Au@C-TiO_2-x catalysts for enhanced photocatalytic mineralization of Acid red 3R under visible light, *J. Hazard. Mater.*, 2020, **391**, 122246.
55 G. S. Shao, X. J. Zhang and Z. Y. Yuan, Preparation and photocatalytic activity of hierarchically mesoporous-macroporous TiO_2-xNx, *Appl. Catal., B*, 2008, **82**, 208–218.
56 G. B. Soares, B. Bravin, C. M. P. Vaz and C. Ribeiro, Facile synthesis of N-doped TiO_2 nanoparticles by a modified polymeric precursor method and its photocatalytic properties, *Appl. Catal., B*, 2011, **106**, 287–294.
57 J. Yu, Q. Li, S. Liu and M. Jaroniec, Ionic-liquid-assisted synthesis of uniform fluorinated B/C-codoped TiO_2 nanocrystals and their enhanced visible-light photocatalytic activity, *Chem.–Eur. J.*, 2013, **19**, 2433–2441.
58 A. K. Chakraborty, S. Ganguli and M. A. Sabur, Nitrogen doped titanium dioxide (N-TiO_2): Electronic band structure, visible light harvesting and photocatalytic applications, *J. Water Proc. engineering*, 2023, **55**, 104183.
59 B. Dai, Ch. Gao, J. Guo, M. Ding, Q. Xu, S. He, Y. Mou, H. Dong, M. Hu, Z. Dai, Y. Zhang, Y. Xie and Z. Lin, A robust pyro-phototronic route to markedly enhanced photocatalytic disinfection, *Nano Lett.*, 2024, **24**, 4816–4825.
60 Y. Wang, J. Zhao, X. Xiong, S. Liu and Y. Xu, Role of Ni^{2+} ions in TiO_2 and Pt/TiO_2 photocatalysis for phenol degradation in aqueous suspensions, *Appl. Catal., B*, 2019, **258**, 117903.
61 J. A. Rengifo-Herrera, K. Pierzchala, A. Sienkiewicz, L. Forró, J. Kiwi and C. Pulgarin, Abatement of organics and *Escherichia coli* by N, S co-doped TiO_2 under UV and visible light. Implications of the formation of singlet oxygen ($^1O_2$) under visible light, *Appl. Catal., B*, 2009, **88**, 398–406.